Bulletin of the Seismological Society of America, Vol. 86, No. 4, pp. 1028–1041, August 1996

The Possibility of Observing Nonlinear Path Effect in Earthquake-Induced Seismic Wave Propagation

by Igor A. Beresnev and Kuo-Liang Wen

Abstract Observations of the dependence of elastic-wave velocities on stress in the lithosphere, ultrasonic modeling, and field experiments using controllable sources reveal that significant nonlinear elastic effects may occur in seismic wave propagation. Theoretical modeling involving nonlinear wave equation shows that the most pronounced and practically observable implication of the nonlinear elasticity in broadband-signal propagation is the gradual enrichment of the spectra in high-frequency components. We check the significance of nonlinear path effects using the strong ground motion data from two accelerograph arrays in Taiwan. The data cover the motions with peak ground accelerations from 1 to 161 Gal (cm/sec^2) and peak surface strains from 10^{-4} to 10^{-7}. The differences between the average spectra of seismic waves recorded by groups of stations separated by distances of 20 to 40 km are examined to identify the possible nonlinear path effect. Mixed results have been obtained. In the SMART2 array, the increase in high-frequency energy is detected in compliance with the theory, which corroborates elastic nonlinearity. On the other hand, in the NCCU array, no symptoms of nonlinear wave propagation are found. Poor signal-to-noise conditions and restrictions imposed by the frequency band of standard instrumentation might be accountable for the negative result.

Introduction

Nonlinear elastic effects in seismic wave propagation are usually ignored in the applications. In fact, it seems as if no efforts have been made to assess their actual magnitude and the possible impact on wave characteristics. Nevertheless, experimental facts suggest that the problem may not be as straightforward. The question of the significance of the nonlinear seismic phenomena has been raised by several groups of investigators over the last decade. Theoretical and laboratory acoustic modeling was done, and experimental investigations using controllable Vibroseis-type sources were carried out, which did bring in the convincing, albeit limited, support for the occurrence of the nonlinear effects.

If the nonlinear seismic effects are pervasive, they should be seen in the strong ground motions produced by earthquakes, where deformations can be large. However, the occasional character of the existing strong-motion data and their broadband frequency content complicate the task of identifying nonlinear effects as compared with controllable-source experiments. On the other hand, controllable sources never provide strains comparable in size with earthquake-induced motions.

The appearance of permanent strong-motion arrays in the recent history of seismological observations provides an opportunity to verify the hypothesis of the significance of nonlinear seismic phenomena. Such an investigation is a subject of this article. In the first section, we give a general overview of nonlinear elasticity in rock and its implications on wave propagation. In the second and third sections, experimental data and the results are presented. In the two final sections, we discuss the results and give the conclusions.

It should be emphasized that the nonlinear response of near-surface sedimentary layers (the nonlinear site effect) is not of concern here. We focus on the path effect, i.e., the propagation phenomena in the bulk of the medium.

Review of the Problem

Nonlinear Elasticity of Rock

The linear theory of elastic waves is valid in the limiting case of infinitesimal deformations. Likewise, the linearity of the constitutive laws for solids is an approximation. The fact that seismic wave velocities tend to depend on the applied stress suggests the rock nonlinearity.

The elementary theory shows (see Appendix) that general expression for the nonlinear stress-strain relationship in the propagating planar wave can be represented as

$$\sigma = \rho_0 c_0^2 \varepsilon \left(1 + \left.\frac{d \ln c}{d\varepsilon}\right|_{\varepsilon=0} \varepsilon\right), \qquad (1)$$

where σ and ε are the stress and strain, respectively; ρ_0 and c_0 are the density and the elastic-wave velocity in the undeformed medium; and c is the wave velocity at arbitrary strain. Equation (1) is valid for both longitudinal and transverse waves and is correct to the second order in strain.

The dimensionless constant

$$\Gamma \equiv \left.\frac{d \ln c}{d\varepsilon}\right|_{\varepsilon=0} \tag{2}$$

is a *nonlinear parameter* that serves as a qualitative measure of the quadratic nonlinearity of the constitutive law. Expression (2) shows that Γ is fully determined by the dependence of seismic wave velocities on strain. The strain-induced changes in velocity are therefore a direct indication of the elastic nonlinearity of a solid.

The one-dimensional equation of motion of an elastic continuum reads

$$\rho_0 \frac{\partial^2 u}{\partial t^2} = \frac{\partial \sigma}{\partial x}, \tag{3}$$

where, assuming a wave-propagation case, u is the displacement in P or S wave (along or perpendicular to the wave propagation direction x, respectively) and σ is the compressional or shear stress. Substituting σ from (1) into (3) and recalling that $\varepsilon = \partial u/\partial x$ (where ε stands for a compressional or shear strain), one gets

$$\frac{\partial^2 u}{\partial t^2} - c_0^2 \frac{\partial^2 u}{\partial x^2} = 2c_0^2 \Gamma \frac{\partial u}{\partial x} \frac{\partial^2 u}{\partial x^2}. \tag{4}$$

Equation (4) is an elementary form of the nonlinear wave equation.

Now we can look at what is known from the experiments. De Fazio *et al.* (1973) report the temporal variations in wave-propagation characteristics associated with the changes in stress in the lithosphere. Velocity variations in tectonically active regions have been proposed as a precursory phenomenon for the nucleation of large earthquakes (Scholz *et al.*, 1973; Whitcomb *et al.*, 1973; Morozova and Nevskiy, 1984; Sadovskii, 1985; Nikolaev, 1986; Karageorgi *et al.*, 1992). Nikolaev (1988, 1989) summarizes that shallow crust deformation of the order of 10^{-8}, caused by the Earth's tides or the earthquake nucleation process, causes the relative change in wave velocity of $\Delta c/c = 10^{-4}$ to 10^{-5}. Having $\Gamma = (dc/d\varepsilon)/c \approx (\Delta c/c)(1/\Delta\varepsilon)$, we find that the corresponding nonlinear parameter has the value of 10^3 to 10^4.

Nonlinear parameter can also be estimated from the laboratory measurements. First, we take the case of nonlinear longitudinal-wave propagation that is often characterized by the five-constant elasticity (Gol'dberg, 1960; Jones and Kobett, 1963). Gol'dberg (1960) uses the five-constant formalism to derive a nonlinear longitudinal-wave equation that coincides with (4) if one assumes that

$$\Gamma = \frac{3}{2} + \frac{A + 3B + C}{\lambda + 2\mu}, \tag{5}$$

where λ and μ are the Lamé's elastic constants and A, B, and C are the third-order elastic moduli. Elastic constants from (5) can be measured in laboratory ultrasonic experiments. The values of Γ for a variety of materials such as water, biological tissues, and polycrystalline metals have the order of $|\Gamma| \leqq 10$ (Zarembo and Krasil'nikov, 1970; Nazarov *et al.*, 1988; Ostrovsky, 1991). On the other hand, rock samples show two- to three-order-of-magnitude higher nonlinearity. Bakulin and Protosenya's (1982) measurements of third-order moduli for crystalline rocks give $|\Gamma| \approx 10^4$. Using a higher-harmonic generation effect in sandstone, Meegan *et al.* (1993) obtain a value of $|\Gamma| = 7.0 \times 10^3 \pm 25\%$.

Second, to estimate the value of the nonlinear parameter in shear waves, we can adapt the data available in geotechnical field. A hyperbolic stress-strain relationship

$$\tau = \frac{\mu_0 \gamma}{1 + \dfrac{\mu_0}{\tau_{\max}} |\gamma|}, \tag{6}$$

where τ and γ are the shear stress and shear strain, respectively; μ_0 is the shear modulus in the undeformed state; and $\tau_{\max}$ is the maximum stress that can be supported by the material, is commonly used in earthquake engineering to characterize the shearing deformation of soils (Hardin and Drnevich, 1972; Yu *et al.*, 1993, equation 7). The expansion of (6) in a binomial series under the assumption of small strain gives an approximation

$$\tau = \mu_0 \gamma \left(1 - \frac{\mu_0}{\tau_{\max}} \gamma\right). \tag{7}$$

Equation (7) coincides with (1) if

$$\Gamma = -\frac{\mu_0}{\tau_{\max}}. \tag{8}$$

The negative value of Γ indicates, according to (2), that shear-wave velocity decreases with increasing strain. This is indeed correct, for velocity reduction at large strains became a geotechnical truism (e.g., Idriss and Seed, 1968, Figs. 3 and 4). The sign of a nonlinear parameter Γ is therefore an important characteristic showing whether the "softening" (velocity decreasing with strain) or "hardening" (velocity increasing with strain) nonlinearity is taking place. The nonlinear parameter for a typical geotechnical soil model can be estimated using the data provided by Yu *et al.* (1993, Fig. 2). At a depth of 20 m in a soil deposit, the shear-wave

velocity $c_{S0} = 300$ m/sec, $\rho_0 = 1800$ kg/m^3, and $\tau_{max} = 10^5$ N/m^2. Thus, equation (8) yields $|\Gamma| \approx 1.6 \times 10^3$.

The laboratory-derived values for longitudinal and transverse waves are in remarkable agreement with the estimates obtained from the *in situ* velocity variations. Thus, different kinds of rock have two- to three-order-of-magnitude larger nonlinear parameters than those generally observed in the nonlinear acoustics. This is explained by the complicated microstructure of the Earth's materials that makes their elastic parameters considerably more dependent on stress conditions.

Effects of Nonlinear Elasticity on Wave Propagation

Equation (4) in the form

$$\frac{\partial^2 u}{\partial t^2} = c_0^2\left(1 + 2\Gamma \frac{\partial u}{\partial x}\right)\frac{\partial^2 u}{\partial x^2} \tag{9}$$

can be regarded as a wave equation with the effective wave velocity of $c_0(1 + 2\Gamma\varepsilon)^{1/2}$, dependent on the local strain. This means that different phases move at different speeds, and only the nodal points propagate with the speed c_0. As a result, the waveform is gradually distorted during propagation. Since the local velocity increment (decrement) is controlled by the quantity $\Gamma\varepsilon$, whether or not distortion has a perceptible value becomes a question of the magnitude of a nonlinear parameter. Assuming the strain of the order of 10^{-4} (which may be produced in the near-source area by a moderate-size earthquake with the local magnitude of about 5, see Tables 1 through 4 below) and $\Gamma = 10^3$, we obtain $\Gamma\varepsilon = 10^{-1}$. Then, from equation (9), a 10% variation in the velocity of the wave phases around the value of c_0 can be anticipated.

In the frequency domain, nonlinear distortion is manifested in the generation of extraneous higher and lower frequencies. To illustrate this point, the approximate solution to equation (4), obtained by a perturbation method, can be considered. Let $u_0(x, t)$ be a solution of a homogeneous equation (4). Following the idea of the method (e.g., Jones and Kobett, 1963), we look for a correction u' to u_0, caused by the presence of a nonlinear term in (4), as a solution of the inhomogeneous equation, where u_0 is substituted into the right-hand side. This leads to the disturbed wave equation

$$\frac{\partial^2 u'}{\partial t^2} - c_0^2 \frac{\partial^2 u'}{\partial x^2} = 2c_0^2\Gamma \frac{\partial u_0}{\partial x}\frac{\partial^2 u_0}{\partial x^2}. \tag{10}$$

We take u_0 as the sum of two sinusoidal waves with the angular frequencies ω_1 and ω_2, the wavenumbers k_1 and k_2, and the amplitudes A_1 and A_2:

$$u_0(x, t) = A_1 \sin(\omega_1 t - k_1 x) + A_2 \sin(\omega_2 t - k_2 x). \tag{11}$$

Substituting (11) into the right-hand side of (10), we get

$$\begin{aligned}\frac{\partial^2 u'}{\partial t^2} - c_0^2 \frac{\partial^2 u'}{\partial x^2} = c_0^2\Gamma\{&A_1^2 k_1^3 \sin 2(\omega_1 t - k_1 x) \\ &+ A_2^2 k_2^3 \sin 2(\omega_2 t - k_2 x) \\ &+ A_1 A_2 k_1 k_2 (k_1 + k_2) \sin[(\omega_1 + \omega_2) \\ &\quad t - (k_1 + k_2)x] \\ &+ A_1 A_2 k_1 k_2 (k_1 - k_2) \sin[(\omega_1 - \omega_2) \\ &\quad t - (k_1 - k_2)x]\}.\end{aligned} \tag{12}$$

The inhomogeneous equation (12) has the "driving" terms at frequencies $2\omega_1$, $2\omega_2$, $\omega_1 + \omega_2$, and $\omega_1 - \omega_2$. They create the new waves with the double, sum, and difference frequencies, respectively, that do not exist at the source and are the product of a nonlinear interaction between the components of the initial wave. One of them (at the sum frequency) is a solution of the equation

$$\begin{aligned}\frac{\partial^2 u'}{\partial t^2} - c_0^2 \frac{\partial^2 u'}{\partial x^2} = &A_1 A_2 c_0^2 \Gamma k_1 k_2 (k_1 + k_2) \\ &\sin[(\omega_1 + \omega_2)t - (k_1 + k_2)x].\end{aligned} \tag{13}$$

In a nondispersive medium, the primary waves at frequencies ω_1 and ω_2 and the new wave at $\omega_1 + \omega_2$ travel at the same speed interacting in resonance; thus, the amplitude of the solution u' can be expected to grow linearly with distance. Looking for the solution in the form $u' = Bx \cos[(\omega_1 + \omega_2)t - (k_1 + k_2)x]$ and substituting it into the left-hand side of (13), one gets $B = -(A_1^2 A_2^2 \Gamma k_1 k_2)/2$, and the solution to (13) becomes

$$\begin{aligned}u'(x, t) = -\frac{A_1^2 A_2^2 \omega_1 \omega_2 \Gamma}{2c_0^2} x \cos[&(\omega_1 + \omega_2) \\ &t - (k_1 + k_2)x].\end{aligned} \tag{14}$$

Similarly treating the other terms in the right-hand side of (12), we conclude that nonlinear interaction between the two primary waves spawns the waves at new frequencies, whose amplitudes grow as the waves propagate. The unlimited amplitude increase is not physical, yet, and originates from the perturbation method itself. In practical situations, attenuation will limit harmonics' growth. However, solution (14) does show the principal consequence of the elastic nonlinearity, which is the generation of new frequencies in wave propagation.

In broadband signals, each individual spectral component produces a second harmonic and a sum and difference with every other component, thus expanding spectrum to both low- and high-frequency ends. This qualitative reasoning is confirmed by the solution of a nonlinear wave equation for the broadband source in the presence of dissipation obtained by McCall (1994). The spatial evolution of displacement and acceleration spectra of a longitudinal pulse is presented in Figure 1. As signal propagates, the sum and difference frequencies are progressively produced. The high-frequency contribution is far more distinct. It can be ex-

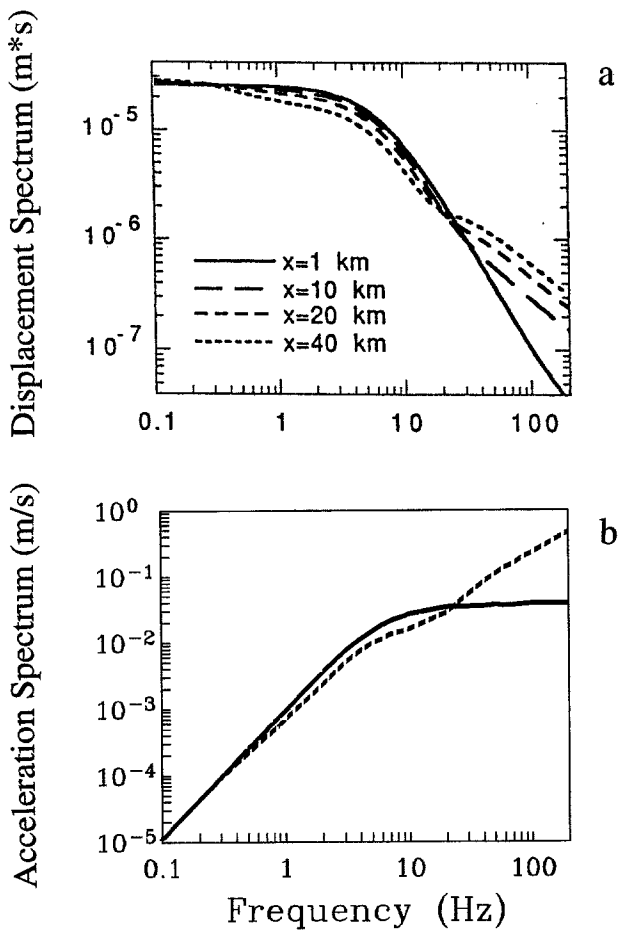

Figure 1. Theoretical spatial alteration of (a) displacement and (b) acceleration spectra from a broadband seismic source in the presence of nonlinearity and attenuation (after McCall, 1994). The pulse propagates to the distances of 1, 10, 20, and 40 km. The assumed unelastic attenuation factor Q is 100. The original displacement spectra were multiplied by ω^2 to get accelerations, and only two extreme curves in (b) have been retained.

pected from Figure 1 that generation of higher harmonics becomes tangible at frequencies much higher than the corner frequency of the source. Note that realistically observed strong-motion acceleration spectra do not grow to the frequencies as high as shown by the dashed line in Figure 1b, decaying beyond a certain frequency f_{max}. The presence of f_{max} presumably takes origin in the near-surface attenuation and scattering processes (e.g., Boore, 1983, p. 1868).

The leakage of energy to lower and higher frequencies is a generic feature of nonlinear wave processes, independent of nature of a particular elastic-wave field. For instance, analogous effects are experimentally observed in the finite-amplitude acoustic pulses in air (Pestorius and Blackstock, 1973).

The pattern shown in Figure 1 can be used as a clue to identifying nonlinear path effect in experimental data analysis.

Existing Experimental Evidence for Nonlinear Path Effects

Nonlinear effects have been extensively studied in the acoustics of solids (Zarembo and Krasil'nikov, 1970). Evidence for nonlinear path effects in the seismic fields has been reported in some instances; however, the number of reliable demonstrations remains scarce. Clearly, the best opportunity to identify nonlinear effects is provided by the study of monochromatic signals, when generation and growth of harmonics with multiple frequencies can be compelling evidence for the significance of nonlinear propagation effect.

Beresnev *et al.* (1986), Beresnev and Nikolaev (1988), and Dimitriu (1990) studied the propagation of single-frequency seismic waves from a Vibroseis-type source up to the distances of several kilometers and noted the significant harmonic distortion effects. The acoustic nonlinearity of rock also has been studied under laboratory conditions by Bonner and Wanamaker (1991), Meegan *et al.* (1993), and Johnson and McCall (1994). The generation of second harmonic in the monochromatic field and broadening of the spectrum of pulse signals have been noted. However, we are not aware of any works where the possible nonlinear contribution to the spectra of earthquake-generated seismic waves has been studied.

Earthquake Data Used

SMART2 Accelerograph Array

We use the strong-motion data recorded by two surface accelerograph arrays in Taiwan. The SMART2 array is currently installed in its east coast (Beresnev *et al.*, 1994) (Fig. 2). The permanent part of the array consists of about 45 stations (solid circles in Fig. 2) and has been in operation since December 1990. Following the 13 December 1990 M_L 6.0 Hualien earthquake with the epicenter at latitude 23°45′ and longitude 121°38′, a part of the SMART2 permanent stations were moved to the south to form a temporary network of 15 stations to document aftershock activity (solid squares in Fig. 2). This temporary array was in place for approximately 1 month. Figure 2 shows that the SMART2 installation combined with the temporary stations has a maximum linear dimension of about 60 km, making the data suitable for the search of nonlinear path effects.

All the stations are equipped with Kinemetrics FBA-23 16-bit three-component accelerometers and the SSR-1 recorders. The pre-event memory was set to 10 sec, and the ground motion was digitized at 200 samples per second. Preprocessing of the accelerograms included baseline subtraction and bandpass filtering between 0.1 and 50 Hz.

Nearly all of the stations in the extended SMART2 array are positioned along the narrow longitudinal valley bordering upon the central range to the west and the slender coastal range or the Pacific coast to the east. The remaining are the six temporary coastal stations that are separated from the valley by the coastal range (stations 3, 5, 6, 11, 13, and 14

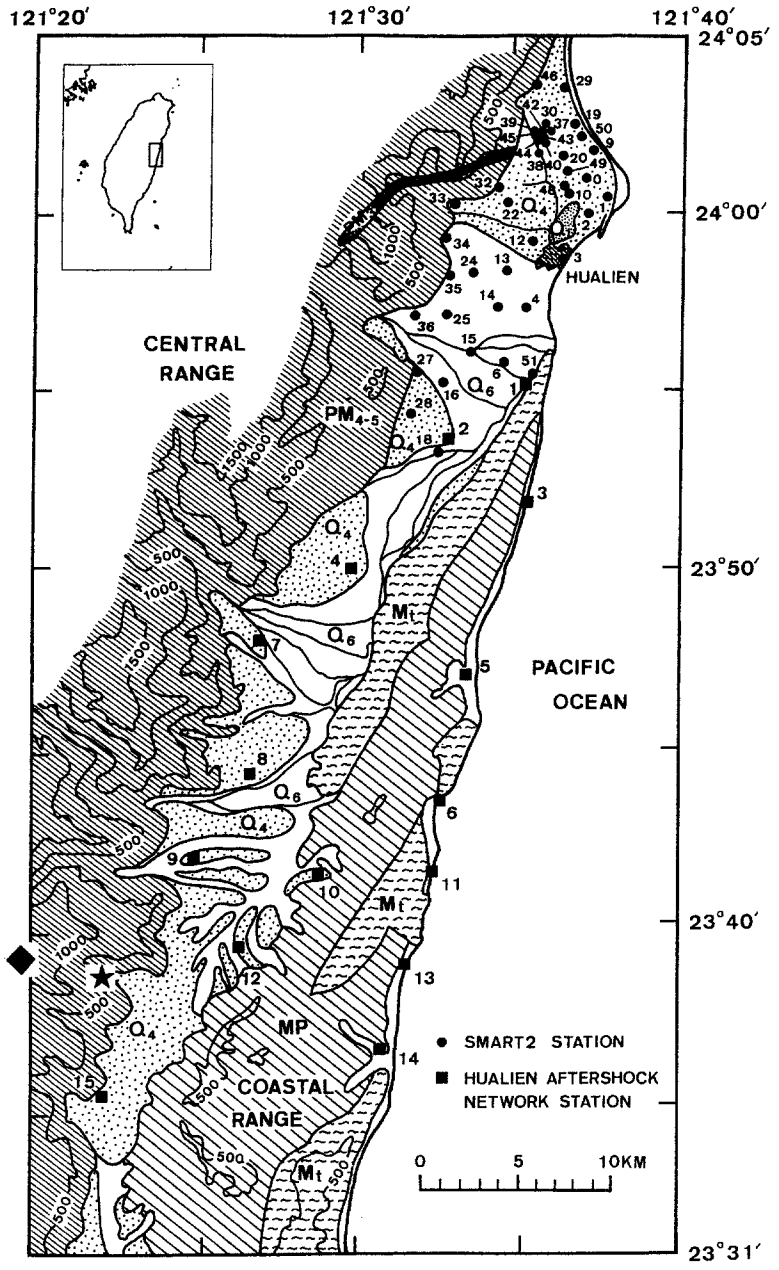

Figure 2. Location and geology of the SMART2 array in Taiwan. Q_6 are the recent alluvium; Q_4 are Pleistocene terrace deposits (gravel, sand, and clay); MP are late Miocene to Pliocene conglomerate, shale, and sandstone; Mt are early Miocene agglomerate and sandstone; and PM_{4-5} is late Paleozoic to Mesozoic schist. The diamond and star stand for the epicenters of earthquakes 67 and 69, respectively.

shown by squares in Fig. 2). The longitudinal valley is a linear depression about 5- to 7-km wide having supposedly a rift origin. Elevations at the SMART2 permanent stations range from 6 m at station 1 to 91 m at station 36, showing a gradual rise from the coast to the central range. Elevations at the temporary network were not registered. All of the stations are either on Pleistocene terrace deposits or on recent alluvium. The borehole drilled to 200 m near station 37 (northern part of the array) through the terrace deposits disclosed four layers (Peng and Wen, 1993). The upper stratum consists of sand with small gravel (0 to 7 m, c_S = 100 m/sec); the second is gravel and mud with some sand (7 to 62 m, c_S = 400 m/sec); the third is sand with clay and small gravel (62 to 150 m, c_S = 460 m/sec); and the fourth layer (below 150 m, c_S = 1060 m/sec) includes rock, pebble gravel, and sand. Bedrock was not reached by a borehole.

Twenty-five aftershocks of the Hualien earthquake with local magnitudes ranging from 3.5 to 5.4 were recorded by an extended array. Representative data of two of them with the position of epicenters and the depth suitable for nonlinear path effect analysis are discussed in a later section.

NCCU Accelerograph Array

The second strong-motion data set comes from the NCCU (National Chung-Cheng University) accelerograph network of about 16 stations deployed over a large area around the cities of Tainan and Chiai in the west coast, which was in place between December 1990 and October 1991

(Fig. 3). Most of the stations were installed in the vast alluvial plain with homogeneous site conditions. Reflection seismic surveys show subhorizontal sedimentary sequences with the depth to the basement of about 1 to 2 km (Yeh *et al.*, 1984, Fig. 2.9). The stations were equipped with the same instrumentation described above.

Figure 3 shows that the maximum spacing between NCCU stations is about 80 km, which makes data appropriate for the path effect studies. Thirty-seven events with local magnitudes from 2.6 to 6.0 were recorded by the array. Typical data from two events with the epicenters shown in Figure 4 are presented below.

Results of Strong-Motion Data Analysis

The SMART2 Array

Figure 1 shows that, to detect nonlinear path effect, one can examine the spectral content of the waves propagating to the sufficiently long distances from the source. In the particular case of the extended SMART2 array, given the general stretch of the network along the longitudinal valley, the study of waves propagating along the valley provides the necessary coverage of epicentral distances. This condition restricts the choice of suitable earthquakes to those lying close to the axis of the valley. From this point of view, events 67 (M_L 4.7) and 69 (M_L 5.1) are the most appropriate ones (event numbers correspond to the SMART2 array catalog). The epicenters of these events, represented by the diamond and star, respectively, are shown in Figure 2.

According to these guidelines, we analyze the changes in spectra of propagating S and P waves that could indicate nonlinear path effect. All the spectra are calculated as follows: (1) a window containing the shear or longitudinal wave is identified; (2) the window is tapered on both ends using a cosine function; (3) the 2048-point Fourier amplitude spectrum is calculated; (4) the spectrum is smoothed 40

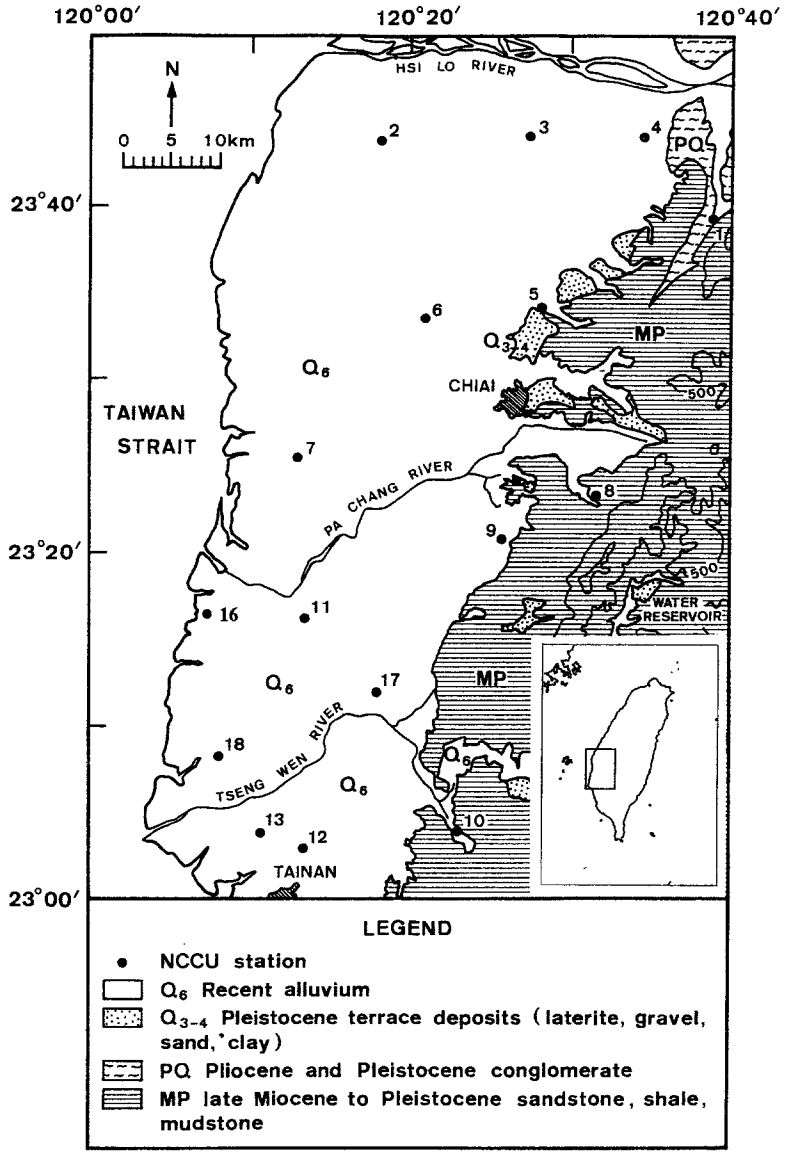

Figure 3. Location and geology of the NCCU array in Taiwan.

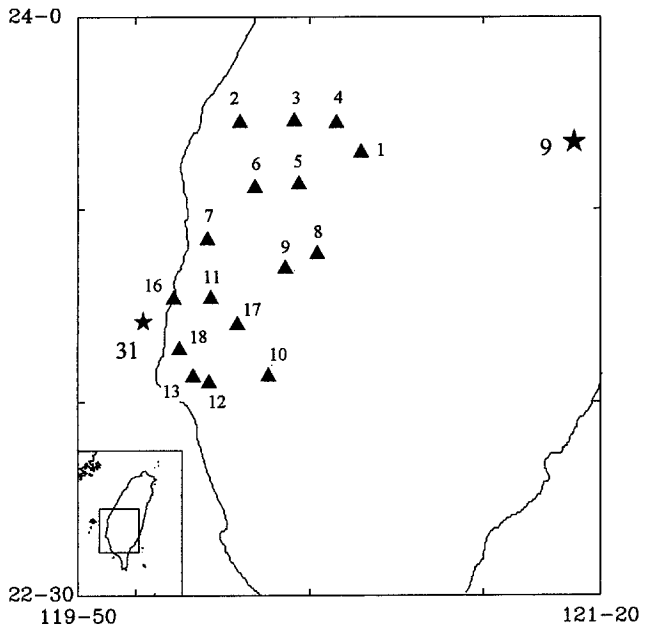

Figure 4. Epicenters of the NCCU earthquakes 9 and 31 (stars) used in the analysis. The triangles stand for the NCCU stations.

times using a three-point running Hanning average. The spectra of P waves are calculated from the vertical component of the accelerograms, while the spectra of S waves are obtained as arithmetic average of those for E–W and N–S components.

The parameters of events 67 and 69 are summarized in Tables 1 and 2, where the value of 500 is added to the numbers of temporary network stations to distinguish them from the permanent SMART2 stations. To calculate peak strains, we use the following approximate formula. In the sinusoidal planar wave $u = U \sin(\omega t - kx)$,

$$\max|\varepsilon| \equiv \max\left|\frac{\partial u}{\partial x}\right| = kU = \frac{A}{2\pi fc}, \qquad (15)$$

where u is the longitudinal or transverse displacement; U and A are the amplitudes of displacement and acceleration, respectively; and $f = \omega/2\pi$. The values of PGA (peak ground acceleration) and the predominant frequencies listed in Tables 1 and 2, as well as $c_p = 1500$ m/sec and $c_S = 300$ m/sec, corresponding to near-surface conditions, were used. Tables 1 and 2 show that surface strains in our study are in the interval of 10^{-6} to 10^{-7} in P waves and 10^{-4} to 10^{-6} in S waves. In McCall's (1994) model, peak strain is about 10^{-6}. Thus, the theoretical results in Figure 1 simulate our field data closely.

The last two columns in Tables 1 and 2 show the frequency intervals where the signal-to-noise ratio (S/N) exceeds the value of 2 (see footnote to Table 1). Strictly speaking, S/N goes down to this value only at the edges of the intervals, whereas it reaches the value of approximately 100 near the dominant frequencies.

In the subsequent analysis, the spectra at near-source ("reference") stations are compared with those at the distant stations to check whether the difference in spectral shape consistent with Figure 1 is seen. The higher-harmonic generation effect is sought in the data.

In the analysis of strong ground motions, the specific data features should be kept in mind. The path effect cannot be as readily isolated from the strong-motion records as it can be in controlled-source experiments. If the stations are near earthquake source, due to finite-source effects, the recordings are affected by the spatial variance in source directivity. In addition, the site response can considerably alter wave spectra. To realize the magnitude of source and site spectral contributions, we compare the average near- and far-field spectra, each being obtained from a group of stations having similar site conditions.

Figure 5 compares P-wave average acceleration spectra of three separated groups of stations, for earthquake 67. Two of them are "close-to-source" stations, and one comprises the distant stations where nonlinear path effect is presumably taking place. In Figure 5a, the average "reference" spectrum calculated from stations 508, 509, 510, and 512 (solid line) is compared with the average distant spectrum for stations 3 and 19 (dashed line). Figure 5b similarly compares the spectrum for stations 506 and 511 (solid line) with the same remote spectrum (dashed line). The hatched bands represent ± 1 standard deviation. The difference in the hypocentral distance between the two groups is 29 to 42 km in Figure 5a and 22 to 30 km in Figure 5b. The theory shows that, for this difference in traveled distance, the high-frequency generation effect can be seen at the remote stations.

The choice of the above groups of stations is dictated by our technique of nonlinear effect detection. Stations 508, 509, 510, and 512 and stations 3 and 19 are installed on approximately similar Q_4 deposits. Stations 506 and 511 are on Q_6 sediments. The condition requiring that the distance between compared groups be large enough to let a significant nonlinear path effect develop is also satisfied. However, among the permanent SMART2 instruments located on Q_4 deposits in the northern part of the array, only stations 3 and 19 have been triggered. That is why no more records are available for the calculation of the distant average spectrum.

In Figure 6, the same data as in Figure 5 are presented for S wave. The first observation made is that the average spectra for stations 508, 509, 510, and 512 have a very large uncertainty at high frequencies (Figs. 5a and 6a, solid lines). This can be entirely attributed to the angular variation in source radiation, for the distance between stations is comparable to the epicentral distance. The variation in spectra is large enough to overshadow any high-frequency generation in the dashed spectra that could result from the nonlinear path effect. Thus, if the reference sites are selected close to the epicenter, the source effect can dominate the spectral shapes. On the other hand, the uncertainty is markedly re-

Table 1
Event 67 Parameters (21/01/1991 01:51 UT; M_L 4.7; Depth 2.6 km)

Station	Hypocentral Distance (km)	PGA in S Wave (Gal)	PGA in P Wave (Gal)	f_D in S Wave (Hz)	f_D in P Wave (Hz)	ε_S	ε_P	Δf_S (Hz)	Δf_P (Hz)
506	24.2	8.2	1.3	3.8	7.8	1×10^{-5}	2×10^{-7}	—	—
508	15.4	25.2	18.4	15.2	8.2	9×10^{-6}	2×10^{-6}	0.5–50	0.5–50
509	10.4	56.2	28.4	19.3	28.7	2×10^{-5}	1×10^{-6}	0.5–50	0.5–50
510	16.3	9.6	3.5	1.9	6.8	3×10^{-5}	6×10^{-7}	0.5–50	0.5–50
511	22.0	6.5	1.3	2.1	3.6	2×10^{-5}	4×10^{-7}	—	—
512	11.4	19.6	6.2	1.8	15.4	6×10^{-5}	4×10^{-7}	0.5–50	0.5–50
3	45.7	3.7	3.5	6.3	14.0	3×10^{-6}	3×10^{-7}	0.5–30	1–30
19	51.9	3.9	1.7	8.6	11.3	2×10^{-6}	2×10^{-7}	—	—

A value of 500 has been added to the numbers of temporary network stations to discern them from the SMART2 permanent stations. PGA (peak ground acceleration) in S wave is calculated from E–W and N–S components; PGA in P wave is calculated from V component. f_D is predominant frequency defined as the abscissa of the maximum ordinate of the smoothed Fourier amplitude spectrum; f_D in S wave is an arithmetic average between the values calculated from E–W and N–S components; f_D in P wave represents V component. ε_S and ε_P are the maximum shear and compressional strains at the ground surface, respectively, estimated from the values provided in this table. Δf_S and Δf_P are the frequency bands where the signal-to-noise ratio (S/N) is greater than 2 in S wave and P wave, respectively. S/N for S wave is obtained as the rms (geometric) average of the ratios of the amplitude spectra between its E–W component and the pre-event noise and N–S component and the pre-event noise. S/N for P wave is obtained as the spectral ratio of its V component to the pre-event noise. A dash means that no pre-event noise record was available.

Table 2
Event 69 Parameters (21/01/1991 18:02 UT; M_L 5.1; Depth 2.8 km)

Station	Hypocentral Distance (km)	PGA in S Wave (Gal)	PGA in P Wave (Gal)	f_D in S Wave (Hz)	f_D in P Wave (Hz)	ε_S	ε_P	Δf_S (Hz)	Δf_P (Hz)
506	22.0	17.6	3.7	3.9	7.7	2×10^{-5}	5×10^{-7}	0.5–40	0.5–40
508	14.4	28.4	28.7	7.7	10.2	2×10^{-5}	3×10^{-6}	0.5–50	0.5–50
509	9.1	86.1	38.9	16.0	28.3	3×10^{-5}	2×10^{-6}	0.5–50	0.5–50
510	14.1	32.0	11.0	4.5	4.9	4×10^{-5}	2×10^{-6}	0.5–50	0.5–50
511	19.4	13.6	2.3	4.1	3.2	2×10^{-5}	8×10^{-7}	0.5–40	0.5–40
512	8.6	45.0	23.2	2.3	11.1	1×10^{-4}	2×10^{-6}	0.5–50	0.5–50
0	49.5	4.8	2.4	6.4	16.1	4×10^{-6}	2×10^{-7}	0.5–40	0.5–40
19	51.7	6.0	3.1	6.5	12.5	5×10^{-6}	3×10^{-7}	—	—
39	50.2	6.4	3.5	7.0	22.1	5×10^{-6}	2×10^{-7}	—	—

See footnote to Table 1.

duced in the average spectra for stations 506 and 511, which are farther from the source (Figs. 5b and 6b, solid lines). Its value for these stations most probably characterizes the slight difference in local site response. The same magnitude of standard deviation is exhibited by the remote spectra (dashed lines) that are also likely to have been caused by the variation in site conditions.

The second observation is that Figures 5b and 6b display higher spectral values at distant stations than at the reference stations at the frequencies above approximately 10 Hz, where the difference between the average spectra is well in excess of the error margin. This general pattern remains the same for both P and S waves. This result is consistent with the nonlinear path effect assumption. We discuss it in more detail later.

Figures 7 and 8 show similar results for the larger-magnitude earthquake 69. In this case, two near-source groups of stations are the same as for earthquake 67, while the distant group is composed of three stations: 0, 19, and 39. The difference in hypocentral distance between stations 508, 509, 510, and 512 and the distant group is in the interval of 35 to 43 km. Similarly, the spacing between groups 506 and 511 and the distant group is between 28 and 32 km.

Figures 7a and 7b compare the average P-wave spectra for the first near-source group and the far-off group and the second near-source group and the far-off group, respectively. Figures 8a and 8b do the same for the S wave. It can be seen that the characteristics of average spectra discussed for event 67 are similar for event 69. Large variations in source directivity in the near field cause the high values of standard deviation for both P and S waves (Figs. 7a and 8a, solid lines). This virtually precludes the use of spectra at stations 508, 509, 510, and 512 as the reference ones. On the other hand, the standard deviations in the average spectra for stations 506 and 511 (second reference group) are significantly lower due to their longer distance from the epicenter (Figs. 7b and 8b, solid lines). They are comparable to the standard deviations at stations 0, 19, and 39 (dashed

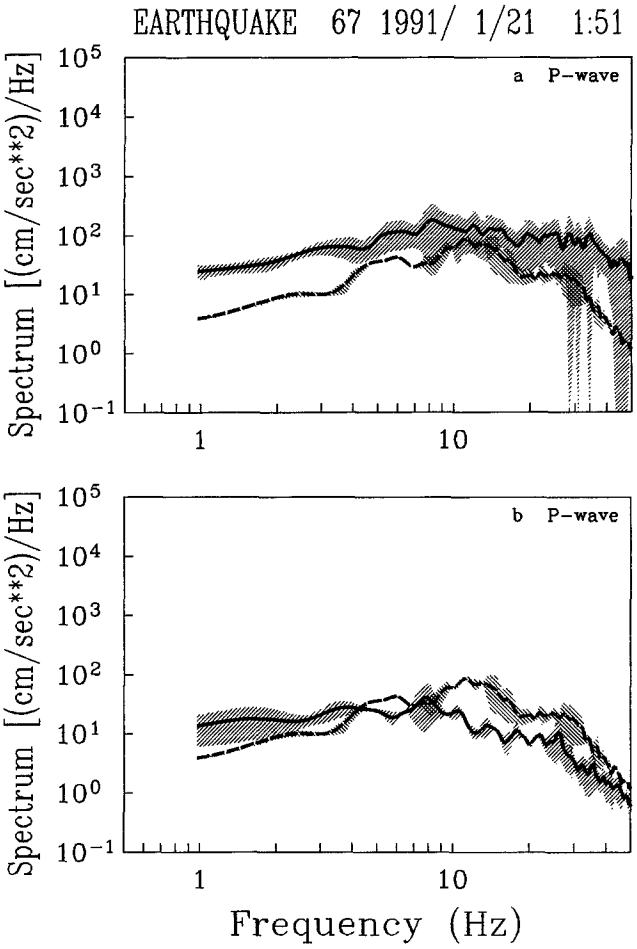

Figure 5. Average *P*-wave acceleration spectra for earthquake 67 calculated from (a) stations 508, 509, 510, and 512 (solid line) and 3 and 19 (dashed line), and (b) from stations 506 and 511 (solid line) and 3 and 19 (dashed line). Hatched areas represent ±1 standard deviation. In both (a) and (b), the solid line is a "reference" near-source spectrum, and the dashed line is a distant spectrum where the nonlinear path effect is theoretically anticipated.

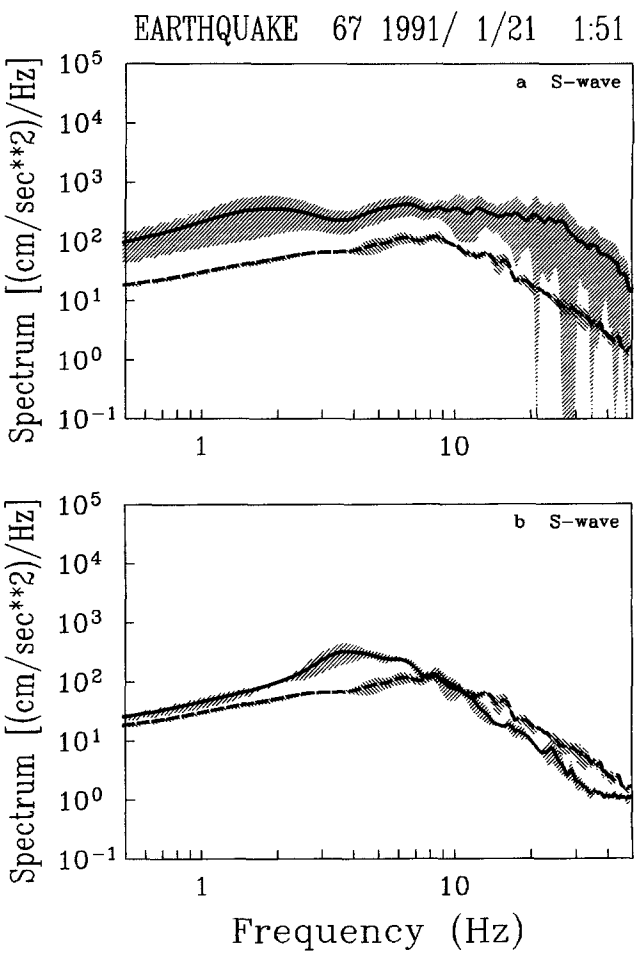

Figure 6. *S*-wave spectra; otherwise the same as Figure 5.

lines). There is no qualitative difference between the behavior of *P* and *S* waves. The apparent high-frequency generation effect is seen in Figures 7b and 8b.

The nonlinearly created harmonics in Figures 5 through 8 appear at frequencies higher than the corner frequency (inferred from the corresponding displacement spectra). From this point of view, the field results match the theory.

The NCCU Array

Following the criteria of the number of triggered stations and the sufficient interstation distance, events 9 (M_L 5.4) and 31 (M_L 4.6) from the NCCU database have been selected. Event numbers correspond to the original NCCU catalog. Their epicenters are shown in Figure 4 and general parameters outlined in Tables 3 and 4. Earthquake 9 produced peak strains of the order of 10^{-6} in *P* wave and 10^{-5} in *S* wave. The strains are 10^{-6} to 10^{-7} and 10^{-4} to 10^{-5}, respectively, for earthquake 31.

The average spectra calculated for stations 1 and 4, and 7 and 11 are compared in Figure 9, where (a) and (b) show the *P*- and *S*-wave spectra, respectively. Stations 1 and 4 are regarded as near-source stations, whereas we look for the possible nonlinear path effect at the farther stations 7 and 11. The minimum differential hypocentral distance between pairs is 42 km, which coincides with the distance yielding the most pronounced nonlinear effect in Figure 1.

Figure 9 displays a regular attenuation with distance and does not make clear any higher-harmonic generation in *P* or *S* wave. The hypocentral distance to all of the stations is of the order of 100 km, making the differential source effect in the spectra negligibly small. Error bands around the curves show a very weak variation in the local site response despite the relatively large distance between the stations. The spectral "hump" between 11 and 19 Hz in Figure 9a (dashed line) is caused by the local resonance at station 7, as was established by a special investigation. It should be noted, though, that the poor S/N conditions at most of the records

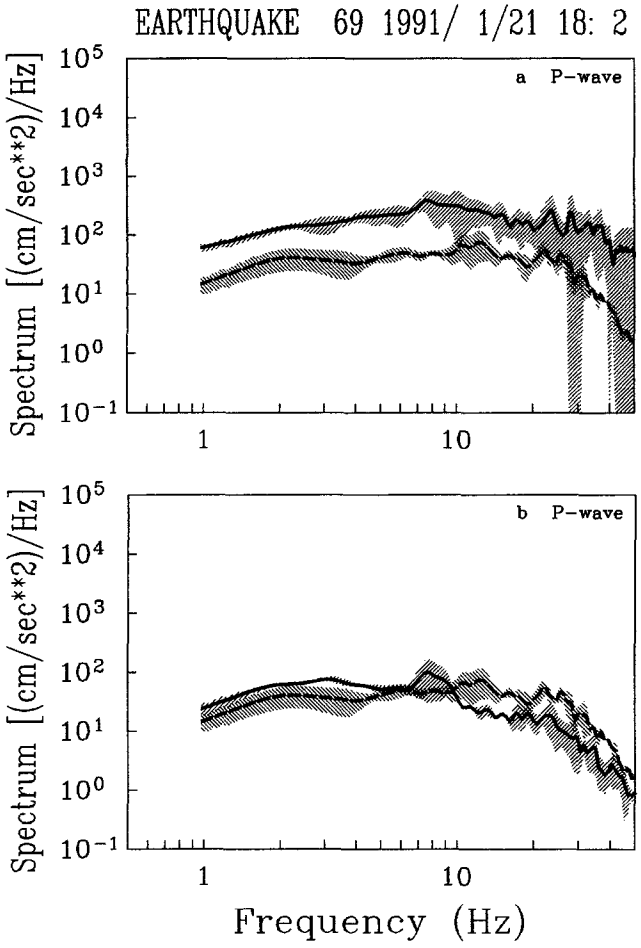

Figure 7. Average acceleration spectra of *P* wave for earthquake 69 calculated from (a) stations 508, 509, 510, and 512 (solid line) and 0, 19, and 39 (dashed line), and (b) from stations 506 and 511 (solid line) and 0, 19, and 39 (dashed line). In both (a) and (b), the solid line is a "reference" near-source spectrum, and the dashed line is a distant spectrum where the nonlinear path effect is theoretically anticipated.

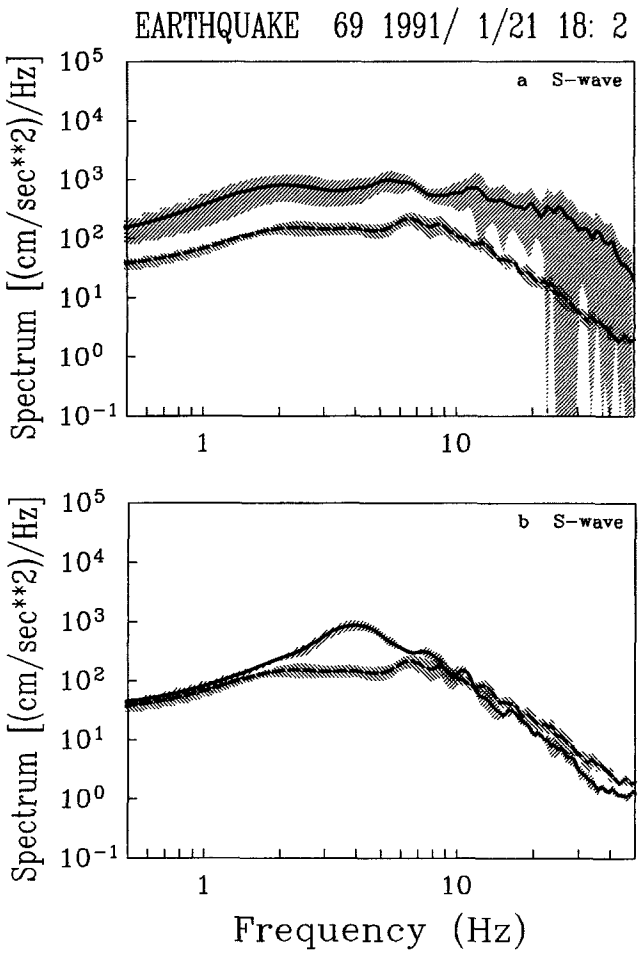

Figure 8. *S*-wave spectra; otherwise the same as Figure 7.

restrict the analysis of high-frequency spectral content to not more than 10 to 20 Hz.

The relatively deep and low-magnitude earthquake 31 occurred in the proximity of station 16, where it produced a large PGA of 161 Gal. However, due to the event's predominantly high-frequency content, PGA attenuated fast to 8.5 Gal at station 6 (Table 4). These two stations have a difference in hypocentral distance of 35 km. They lie on approximately the same azimuthal line to epicenter, which permits the supposition that the differential source effect does not affect them considerably. In addition, they have a favorable working frequency range extending to 40 Hz at remote station 6.

Figure 10 shows the spatial evolution of the *P*- and *S*-wave spectra of event 31 from station 16 to station 6. Spectra at both sites have a similar shape and exhibit a strong attenuation. No high-frequency generation effect is seen in the entire frequency range. It should be kept in mind, however, that the corner frequency of the displacement spectra is around 10 Hz (for *P* wave), as observed at station 16. This implies that the nonlinearly generated harmonics could appear beyond the usable frequency band.

Discussion

Theoretical estimates based on the observed nonlinear elastic properties of rock show that nonlinear path effects in seismic wave propagation can develop to observable quantities and tangibly alter the spectra of *P* and *S* waves. Laboratory and field experiments employing controllable sources substantiate this hypothesis.

It is clear, however, that major obstacles exist in identifying nonlinear path effect from the real earthquake data. First, these data are generally collected by the quasipermanent arrays, and, given the random appearance of earthquakes in space and time, the ideal configuration for detecting the path effect cannot be achieved. Second, the spectra of strong seismic motions are contaminated by the spatially varying source and site effects that may well exceed the

Table 3
Event 9 Parameters (18/01/1991 01:37 UT; M_L 5.4; Depth 0.8 km)

Station	Hypocentral Distance (km)	PGA in S Wave (Gal)	PGA in P Wave (Gal)	f_D in S Wave (Hz)	f_D in P Wave (Hz)	ε_S	ε_P	Δf_S (Hz)	Δf_P (Hz)
1	63.1	14.4	2.9	1.3	1.6	6×10^{-5}	2×10^{-6}	0.5–20	0.5–40
4	70.3	15.6	5.4	1.3	1.3	6×10^{-5}	4×10^{-6}	0.5–10	0.5–10
7	112.0	8.9	3.0	2.2	1.2	2×10^{-5}	3×10^{-6}	0.5–20	0.5–20
11	116.7	7.5	1.9	1.3	1.0	3×10^{-5}	2×10^{-6}	—	—

See footnote to Table 1.

Table 4
Event 31 Parameters (22/03/1991 06:08 UT; M_L 4.6; Depth 13.3 km)

Station	Hypocentral Distance (km)	PGA in S Wave (Gal)	PGA in P Wave (Gal)	f_D in S Wave (Hz)	f_D in P Wave (Hz)	ε_S	ε_P	Δf_S (Hz)	Δf_P (Hz)
6	52.5	8.5	2.8	6.5	21.1	7×10^{-6}	1×10^{-7}	0.5–50	1–40
16	17.6	161.3	20.6	7.3	25.6	1×10^{-4}	9×10^{-7}	0.5–50	0.5–50

See footnote to Table 1.

magnitude of the phenomenon sought for. In the present study, we tried to estimate their value by combining the nearby stations installed on similar type of ground into groups, assuming that error estimates for the average spectra characterize the source and site-effect contribution. The groups separated by the sufficiently long distances are then compared to assess the path effect. Nevertheless, this technique is not capable of isolating it completely. Third, real data contain noise. Earthquake signals are bandlimited, with the signal-to-noise ratio falling off rapidly toward the ends of the usable frequency interval. The high-frequency limit beyond which S/N drops below the value of 2 in our investigation is 10 to 40 Hz at the remote stations. This substantially restrains the capability of detecting the higher-harmonic generation. Finally, the standard strong-motion instrumentation used has its highest recorded frequency equal to 50 Hz. At the same time, theoretical calculation in Figure 1 shows that the high-frequency generation by elastic nonlinearity is visible beyond the crossover of about 30 Hz and becomes discernible at frequencies above 40 to 50 Hz, given the corner frequency of the source of about 3 to 4 Hz. Obviously, these crossovers are at the very edge of the capabilities imposed by the S/N for the moderately strong earthquake and the frequency band of the standard equipment.

Assuming that the source effects are reduced by taking the second near-source group of stations as the reference, Figures 5b, 6b, 7b, and 8b demonstrate an apparent leakage of energy to frequencies higher than the corner frequency as the signal propagates. This result appears in both P and S waves. However, this observation needs to be carefully interpreted. Attributing this phenomenon to nonlinear path effect may be correct if alternative explanations can be shown improbable. For instance, the observed behavior of average spectra can originate in the common peculiarities of a site response at reference stations 506 and 511 or the remote stations. Two facts play down the validity of this hypothesis. First, the stations in each group are at a distance of at least several kilometers from each other, which rules out the possibility of a local resonance affecting the result. Second, our previous study shows that the spectral ratio between the Q_4 and Q_6 sediments is below unity above 10 to 20 Hz for a large number of small earthquakes; i.e., the amplitudes at alluvium sites are amplified over the amplitudes at the terrace deposit sites (Beresnev *et al.*, 1995, Figs. 10 and 15). We see just the reverse of that in Figures 5b, 6b, 7b, and 8b, which can be explained by a nonlinear path effect contributing to the amplitude growth at high frequencies.

Another point is that the same observation sustains for the two different earthquakes 67 and 69, supporting the hypothesis that the nonlinear path effect has been detected. The strains developed in P wave at stations 506 and 511 are 5×10^{-7} and 8×10^{-7}, respectively, in earthquake 69, which makes them comparable to the value of 10^{-6} in McCall's (1994) numerical simulation. Johnson and McCall (1994), on considering ultrasonic modeling, infer that the deformations as low as 10^{-7} are large enough to produce a detectable nonlinear response at large distance from the seismic source. Thus, the effect in our study is compatible with both theoretical results and laboratory modeling.

Another alternative explanation may lie in the fact that the waves from earthquakes 67 and 69 cross the complex geologic structure beneath the longitudinal valley before they reach stations 506 and 511, whereas they propagate along the valley toward the far-off stations 0, 3, 19, and 39. This may have resulted in an anomalously high attenuation of high frequencies in the valley-crossing waves and, consequently, the reduction in their spectral amplitudes with respect to the remote stations. In an attempt to preclude this result, we examined the waves from the other earthquakes

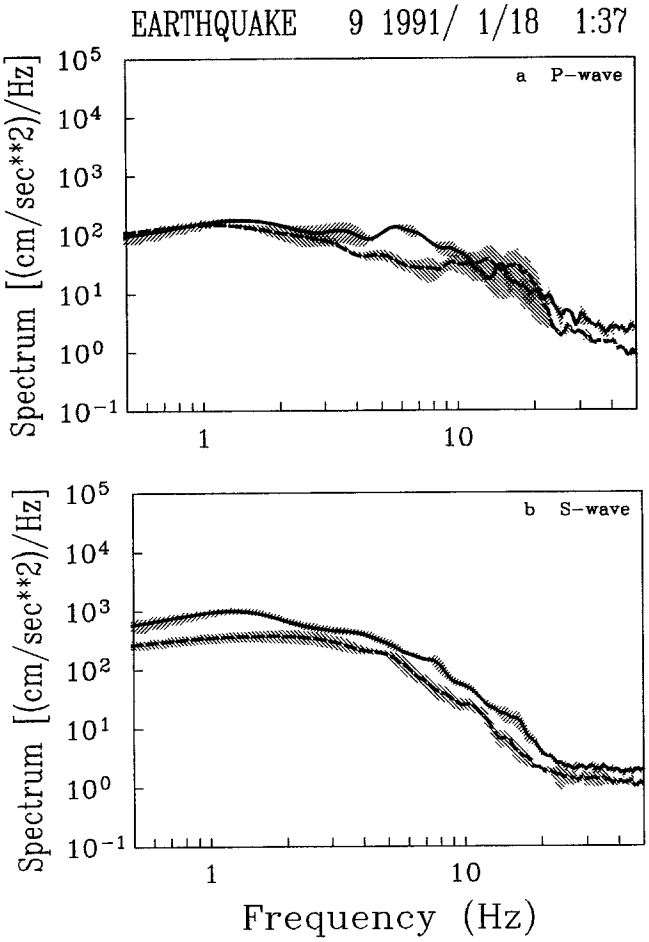

Figure 9. Average acceleration spectra of earthquake 9 calculated from stations 1 and 4 (solid lines), and 7 and 11 (dashed lines) for (a) *P* wave and (b) *S* wave. Solid lines represent the reference spectra; dashed lines are the distant spectra.

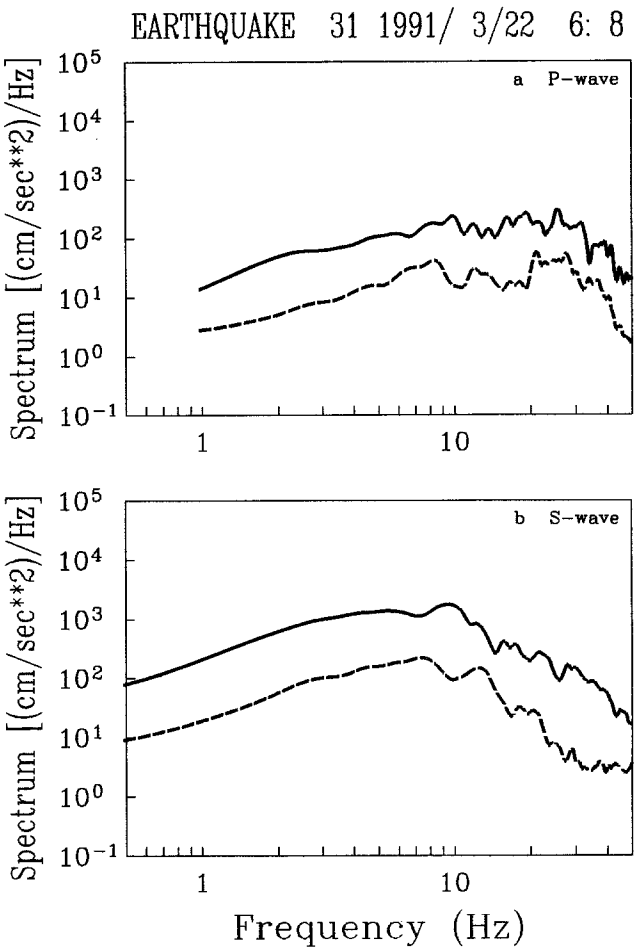

Figure 10. Acceleration spectra of earthquake 31 at stations 16 (solid lines) and 6 (dashed lines) for (a) *P* wave and (b) *S* wave.

with epicenters off the coast crossing the valley in the opposite direction and did not find their elevated attenuation relative to the waves traveling along the coast. However, another fact that needed to be explained is that the average spectra in Figures 5a, 6a, 7a, and 8a, where another near-source group of stations is taken as a reference point, do not show any signs of nonlinear path phenomena. The argument explaining that the source effect prevails in near-field spectra and causes their unusually large standard deviation alleviates this problem.

The effects of scattering and attenuation should also be considered in this discussion. The dissipation of energy, increasing with frequency, works against harmonic distortion. If nonlinear effects had not been present, the dissipation would have destroyed the high spectral components seen. The effect of scattering, which also increases with frequency, may cause transferring high-frequency energy to later arrivals as wave propagates. If this effect were strong, we could see a decrease in high-frequency components in *P* waves and their boost in *S* waves, or a simultaneous decrease in both types of waves. Instead, an increase in high-frequency components is observed in both *P* and *S* waves. The assumption of a nonlinear harmonic distortion provides an explanation for this fact.

In a summation of all aspects, the hypothesis on the possible detection of the nonlinear path effect in wave propagation to the distances of 20 to 40 km has been corroborated as a result of the SMART2 data analysis.

This statement would be less affirmative if only the NCCU data were considered. The NCCU array provides the records from the stations located in a more tectonically homogeneous area with uniform site characteristics. Despite this and the rather high level of strains achieved in earthquakes 9 and 31, no symptoms of nonlinear elastic effects have been revealed (Figs. 9 and 10). This may lead to a corroboration of the linear wave-propagation characteristics; however, the close scrutiny of the data provides a possible explanation for the negative result as well. First, the poor signal-to-noise ratio for most of the records of earthquake 9, which occurred relatively far from the array, has been noted already. As Table 3 shows, frequencies higher than 10 to 20 Hz, where nonlinear effect is likely to take place, are hardly reliable. Second, earthquake 31 produced a good S/N but is

enriched in high frequencies at the source, with a corner frequency of about 10 Hz. In these circumstances, the nonlinearly created harmonics, according to theoretical results, should appear at frequencies beyond 40 to 50 Hz that cannot be addressed in these data. With this taken into account, the negative result regarding the observation of nonlinear path effect at the NCCU array cannot be considered as conclusive.

The following criteria have to be satisfied in future studies. First, the apparatus should allow the analysis of the frequencies higher than 50 Hz. Second, large strains of not less than 10^{-3} to 10^{-5} should be considered. Third, configuration of seismic stations should cover the distances from the source to 40 to 60 km, and all of them should be installed on a similar type of ground to exclude site-response variations.

Conclusions

We developed a technique permitting an assessment of source and site effects and the isolation of possible nonlinear path effect in strong ground motion propagation. The examination of data from two surface arrays in Taiwan provided mixed results. After considering possible alternative explanations, we conclude that the amplification of high frequencies revealed from the spectra of remote stations at the SMART2 array is caused by the nonlinear wave-propagation phenomena. The effect is compatible with that deduced from the numerical modeling involving nonlinear wave equation. At the same time, no effect was found from the records of the NCCU array, despite the more favorable geological setting. Restrictions imposed by the signal-to-noise ratio and the frequency range of standard recording equipment may be responsible for the negative result.

Acknowledgments

We thank Dr. H.-C. Chiu and the technical staff of the Institute of Earth Sciences (IES) who are in charge of the operation of the SMART2 array. Dr. K.-B. Ou of the National Chung-Cheng University kindly provided the data of the NCCU array. Corrected SMART2 accelerograms were prepared at IES by W. G. Huang and the data processing group. We are indebted to A. McGarr and the two anonymous reviewers for their helpful comments. This work was supported by the National Science Council, Republic of China, under Grant NSC 83-0202-M-001-004.

References

Bakulin, V. N. and A. G. Protosenya (1982). Nonlinear effects in travel of elastic waves through rocks, *Trans. (Doklady) USSR Acad. Sci., Earth Sci. Sections* **263,** 314–316 (English translation).

Beresnev, I. A., A. V. Nikolayev, V. S. Solov'yev, and G. M. Shalashov (1986). Nonlinear phenomena in seismic surveying using periodic vibrosignals, *Izvestiya Acad. Sci. USSR, Fiz. Zemli (Phys. Solid Earth)* **22,** 804–811 (English translation).

Beresnev, I. A. and A. V. Nikolaev (1988). Experimental investigations of nonlinear seismic effects, *Phys. Earth Planet. Interiors* **50,** 83–87.

Beresnev, I. A., K.-L. Wen, and Y. T. Yeh (1994). Source, path, and site effects on dominant frequency and spatial variation of strong ground motion recorded by SMART1 and SMART2 arrays in Taiwan, *Earthquake Eng. Struct. Dyn.* **23,** 583–597.

Beresnev, I. A., K.-L. Wen, and Y. T. Yeh (1995). Nonlinear soil amplification: its corroboration in Taiwan, *Bull. Seism. Soc. Am.* **85,** 496–515.

Bonner, B. P. and B. J. Wanamaker (1991). Acoustic nonlinearities produced by a single macroscopic fracture in granite, in *Review of Progress in Quantitative Nondestructive Evaluation,* Vol. 10B, D. O. Thompson and D. E. Chimenti (Editors), Plenum Press, New York, 1861–1867.

Boore, D. M. (1983). Stochastic simulation of high-frequency ground motions based on seismological models of the radiated spectra, *Bull. Seism. Soc. Am.* **73,** 1865–1894.

Bullen, K. E. (1963). *An Introduction to the Theory of Seismology,* 3rd ed., Cambridge University Press, Cambridge.

De Fazio, T. L., K. Aki, and J. Alba (1973). Solid earth tide and observed change in the *in situ* seismic velocity, *J. Geophys. Res.* **78,** 1319–1322.

Dimitriu, P. P. (1990). Preliminary results of vibrator-aided experiments in non-linear seismology conducted at Uetze, F. R. G., *Phys. Earth Planet. Interiors* **63,** 172–180.

Gol'dberg, Z. A. (1960). Interaction of plane longitudinal and transverse elastic waves, *Soviet Phys. Acoust.* **6,** 307–310 (English translation).

Hardin, B. O. and V. P. Drnevich (1972). Shear modulus and damping in soil: measurement and parameter effects, *J. Soil Mech. Foundations Div. ASCE* **98,** 603–624.

Idriss, I. M. and H. B. Seed (1968). An analysis of ground motions during the 1957 San Francisco earthquake, *Bull. Seism. Soc. Am.* **58,** 2013–2032.

Johnson, P. A. and K. R. McCall (1994). Observation and implications of nonlinear elastic wave response in rock, *Geophys. Res. Lett.* **21,** 165–168.

Jones, G. L. and D. R. Kobett (1963). Interaction of elastic waves in an isotropic solid, *J. Acoust. Soc. Am.* **35,** 5–10.

Karageorgi, E., R. Clymer, and T. V. McEvilly (1992). Seismological studies at Parkfield. II. Search for temporal variations in wave propagation using Vibroseis, *Bull. Seism. Soc. Am.* **82,** 1388–1415.

McCall, K. R. (1994). Theoretical study of nonlinear elastic wave propagation, *J. Geophys. Res.* **99,** 2591–2600.

Meegan, G. D., Jr., P. A. Johnson, R. A. Guyer, and K. R. McCall (1993). Observations of nonlinear elastic wave behavior in sandstone, *J. Acoust. Soc. Am.* **94,** 3387–3391.

Morozova, L. A. and M. V. Nevskiy (1984). Temporal variations in the deformation and velocity of seismic waves in the earth's crust in seismically active regions, *Trans. (Doklady) USSR Acad. Sci., Earth Sci. Sections* **278,** 834–838 (English translation).

Nazarov, V. E., L. A. Ostrovsky, I. A. Soustova, and A. M. Sutin (1988). Nonlinear acoustics of micro-inhomogeneous media, *Phys. Earth Planet. Interiors* **50,** 65–73.

Nikolaev, A. V. (Editor) (1986). *Seismic Monitoring of the Earth's Crust (Seismicheskiy Monitoring Zemnoy Kory),* Nauka, Moscow, 1–286 (in Russian).

Nikolaev, A. V. (1988). Problems of nonlinear seismology, *Phys. Earth Planet. Interiors* **50,** 1–7.

Nikolaev, A. V. (1989). Scattering and dissipation of seismic waves in the presence of nonlinearity, *Pageoph* **131,** 687–702.

Ostrovsky, L. A. (1991). Wave processes in media with strong acoustic nonlinearity, *J. Acoust. Soc. Am.* **90,** 3332–3337.

Peng, H.-Y. and K.-L. Wen (1993). Downhole instrument orientations and near surface Q analysis from the SMART2 array data, *Terrestrial, Atmospheric and Oceanic Sciences (Taiwan)* **4,** 367–380.

Pestorius, F. M. and D. T. Blackstock (1973). Propagation of finite-amplitude noise, in *Finite-Amplitude Wave Effects in Fluids.* Proceedings of the 1973 Symposium, L. Bjorno (Editor), IPC Science and Technology Press Ltd.

Sadovskii, M. A. (Editor) (1985). *Physics of the Earthquake Focus. Part III. Techniques and Some Results of Field Studies,* Oxonian Press Pvt. Ltd., New Delhi, 169–250 (English translation).

Scholz, C. H., L. R. Sykes, and Y. P. Aggarwal (1973). The physical basis for earthquake prediction, *Science* **181,** 803–810.

Whitcomb, J. H., J. D. Garmany, and D. L. Anderson (1973). Earthquake prediction: variation of seismic velocities before the San Fernando earthquake, *Science* **180,** 632–635.

Yeh, Y. T., K.-L. Wen, and Y.-B. Tsai (1984). Seismic risk evaluation on the possible sites for Taiwan Power Company's base loading power plant, Report ASIES-ER8417, Institute of Earth Sciences, Academia Sinica, Taiwan, 1–96.

Yu, G., J. G. Anderson, and R. Siddharthan (1993). On the characteristics of nonlinear soil response, *Bull. Seism. Soc. Am.* **83,** 218–244.

Zarembo, L. K. and V. A. Krasil'nikov (1970). Nonlinear phenomena in the propagation of elastic waves in solids, *Soviet Phys. Uspekhi* **13,** 778–797 (English translation).

Appendix

The stress-strain relationship in a linear elastic material reads

$$\sigma_{ij} = \lambda\theta\delta_{ij} + 2\mu\varepsilon_{ij}, \tag{A1}$$

where σ_{ij} is the stress tensor, $\varepsilon_{ij} = 1/2[(\partial u_i/\partial x_j) + (\partial u_j/\partial x_i)]$ is the linearized strain tensor, u_i is the ith displacement component, δ_{ij} is the Kronecker symbol, λ and μ are the Lamé's elastic constants, and $\theta = \partial u_i/\partial x_i$ (in the form using a summation convention) (Bullen, 1963, equation 32). If the deformation in a compressional planar wave traveling along the x axis is considered, then (A1) is rewritten as

$$\sigma_{xx} = (\lambda + 2\mu)\frac{\partial u_x}{\partial x} = (\lambda + 2\mu)\varepsilon_{xx} = \rho c_P^2 \varepsilon_{xx}, \tag{A2}$$

where ρ is the density and c_P is the longitudinal wave velocity. One can generalize, therefore, that in the planar-wave case

$$\sigma = \rho c_P^2 \varepsilon, \tag{A3}$$

implying that σ is the compressional stress and that ε is the dilatational deformation.

Now a general case of the nonlinear one-dimensional compressional deformation $\sigma = \sigma(\varepsilon)$ with $\sigma(0) = 0$ can be considered. Using its Taylor expansion in the vicinity of $\varepsilon = 0$ and keeping the terms to the second order in the strain, one gets

$$\sigma(\varepsilon) = \left.\frac{d\sigma}{d\varepsilon}\right|_{\varepsilon=0} \varepsilon + \frac{1}{2}\left.\frac{d^2\sigma}{d\varepsilon^2}\right|_{\varepsilon=0} \varepsilon^2. \tag{A4}$$

From (A3), $\left.\dfrac{d\sigma}{d\varepsilon}\right|_{\varepsilon=0} = \rho c_{P0}^2$, and (A4) becomes

$$\sigma = \varepsilon\rho_0 c_{P0}^2 \left(1 + \frac{1}{2}\left.\frac{\dfrac{d}{d\varepsilon}(\rho c_P^2)}{\rho c_P^2}\right|_{\varepsilon=0} \varepsilon\right), \tag{A5}$$

where ρ_0 and c_{P0} are the undisturbed density and P-wave velocity. In (A5),

$$\left.\frac{d}{d\varepsilon}(\rho c_P^2)\right|_{\varepsilon=0} = \left.\left(c_P^2\frac{d\rho}{d\varepsilon} + 2\rho c_P\frac{dc_P}{d\varepsilon}\right)\right|_{\varepsilon=0}. \tag{A6}$$

Acknowledging $\rho = m/V$, where m and V are the mass and the volume of the deformed element, and taking into account the conservation of mass, $d\rho = (Vdm - mdV)/V^2 = -(m/V)(dV/V) = -\rho\varepsilon$. Consequently,

$$\left.\frac{d\sigma}{d\varepsilon}\right|_{\varepsilon=0} = -\left.\left(\rho\frac{\varepsilon}{d\varepsilon}\right)\right|_{\varepsilon=0} = 0.$$

Then (A6) yields

$$\left.\frac{d}{d\varepsilon}(\rho c_P^2)\right|_{\varepsilon=0} = 2\left.\left(\rho c_P\frac{dc_P}{d\varepsilon}\right)\right|_{\varepsilon=0}, \tag{A7}$$

and, from (A5) and (A7),

$$\begin{aligned}\sigma &= \rho_0 c_{P0}^2\varepsilon\left(1 + \left.\frac{\dfrac{dc_P}{d\varepsilon}}{c_P}\right|_{\varepsilon=0}\varepsilon\right)\\ &= \rho_0 c_{P0}^2\varepsilon\left(1 + \left.\frac{d\ln c_P}{d\varepsilon}\right|_{\varepsilon=0}\varepsilon\right).\end{aligned} \tag{A8}$$

Similarly, recalling that $\tau = \mu\gamma = \rho c_S^2\gamma$, where τ and γ are the shear stress and strain, respectively, and c_S is the shear-wave velocity, the symmetric expression for the shear stress results in

$$\tau = \rho_0 c_{S0}^2\gamma\left(1 + \left.\frac{d\ln c_S}{d\gamma}\right|_{\gamma=0}\gamma\right). \tag{A9}$$

Thus, the final expression for the nonlinear stress-strain relationship valid to the second order in strain is

$$\sigma = \rho_0 c_0^2\varepsilon\left(1 + \left.\frac{d\ln c}{d\varepsilon}\right|_{\varepsilon=0}\varepsilon\right), \tag{A10}$$

where σ and ε stand for either compressional or shear stress and strain, respectively.

Department of Earth Sciences
Carleton University
1125 Colonel By Drive
Ottawa, Ontario K1S 5B6
Canada
(I.A.B.)

Institute of Earth Sciences
Academia Sinica
P.O. Box 1-55
Nankang, Taipei 11529
Taiwan
(K.-L.W.)

Manuscript received 23 January 1995.